Filz, Günther H.; Elmas, Serenay; Markou, Athanasios A.

The structural geometry of a beam element from 4 torqued strips

Published in:
Structures and Architecture

DOI:
10.1201/9781003023555-19

Published: 08/07/2022

Document Version
Peer-reviewed accepted author manuscript, also known as Final accepted manuscript or Post-print

Please cite the original version:
Filz, G. H., Elmas, S., & Markou, A. A. (2022). The structural geometry of a beam element from 4 torqued strips. In P. J. S. Cruz, & M. F. Hvejsel (Eds.), *Structures and Architecture : A Viable Urban Perspective?* (pp. 150-158). CRC Press. https://doi.org/10.1201/9781003023555-19

The structural geometry of a beam element from 4 torqued strips

G. H. Filz
Aalto University, Finland, ENG | Department of Civil Engineering ° ARTS | Department of Architecture

S. Elmas
Aalto University, Finland, ENG | Department of Civil Engineering ° ARTS | Department of Architecture

A. A. Markou
Aalto University, Finland, ENG | Department of Civil Engineering

ABSTRACT: When assembling a tube from 4 identical, thin-walled, flexible, rectangular strips, which are hinge-joined along their longitudinal edges, a hollow, square cross-section is generated. One option for restraining the tube´s 1-DOF-mechanism around its longitudinal axis is to cross-wisely connect its ends at a common seamline. This procedure causes a twist of 90° and sideward shifts of each of the four strips. We provide a description and comparison of the structural geometry of such beam elements. Our investigations are based on physical prototypes, photogrammetric reconstruction, and computational simulations. The beam´s geometrical stiffness, paralleled with its ease of fabrication and assembly opens new avenues for the design of lightweight structures, firstly used in the realization of the kinematic Zero Gravity pavilion at Aalto University.

1 INTRODUCTION

Our recent research interests in lightweight, architectural design and investigations focus on bending-active torsional structures with regards to its selforganized geometry, structural and architectural potentials, limits and qualities. In the field of structural engineering, torsion usually is defined as the act of turning or twisting, or the result of being twisted. The twisting or wrenching of a body by the exertion of a lateral force tends to turn one end or part of it about a longitudinal axis, while the other is fixed or turned in the opposite direction. Vice versa, when a torque is applied to the structure, it will twist along the long axis (Holmes, 2020). However, rotation, twist, and torsion are often used interchangeably for explaining.

Twisted elements and structures such as the Saint John Lateran columns from the 13th century (Tronzo, 2005) (Fuchs, 1951), the Saint Severin Cathedral columns from 1520 (Ayers, 2004), Antoni Gaudi`s unassembled columns for the Colonia Guell (Cornet, 1970) (Tomlow, 2004) or the BMW Museum, Munich by Coop Himmelblau (Werner, 2009) have been realized many times throughout architectural history. This approach can be described as purposely shaped for functional reasons as well as ornamental ones. Besides the aspects of design and aesthetics, in some cases a structural benefit might be inherent. However, bending-active torsional elements and structures are different from many perspectives. Usually, torsion has not been considered beneficial for both, the material and structural aspects (Wise, 2016). Depending on the flexibility of the material, (here intentionally) applied forces twist the thin sheet material, which causes a 90° torsion and therefore residual stresses. In return, the distributed stresses result in unique equilibrium states and shapes, which can be both highly efficient in material use and structural performance as our studies indicate. In this context, the structural geometry of a beam element from 4 torqued, rectangular strips, as it was used for our realized research pavilion "Zero Gravity" (Filz et al., 2019) (Figure 1), is presented. Based on physical prototypes, photogrammetric reconstruction and computational simulations, we provide a description and comparison of the above-mentioned shape in terms of geometry and structural performance for a predefined set-up.

Figure 1 top left: “Zero Gravity” pavilion, a full-scale, kinematic prototype using cantilevering beam elements assembled from 4 identical, rectangular, torqued plywood-strips [photo by G. Filz].

Figure 2 bottom left: Principle of assembling a tube from 4 identical, thin-walled, rectangular strips (a), which are hinge-joined along their longitudinal edges (b). By torqueing the four strips (c, d), a crosswise connection of the tube`s ends is achieved (e), which is re-straining the 1-DOF-mechanism.

Figure 3 bottom right: Geometry of shifted points during assembly

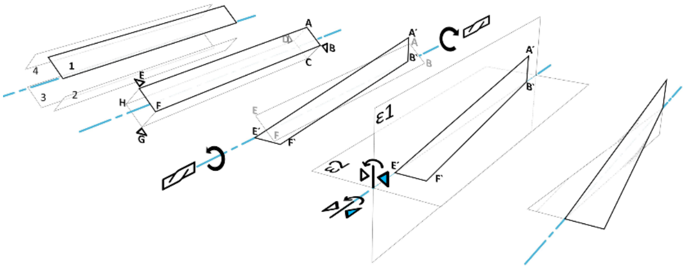

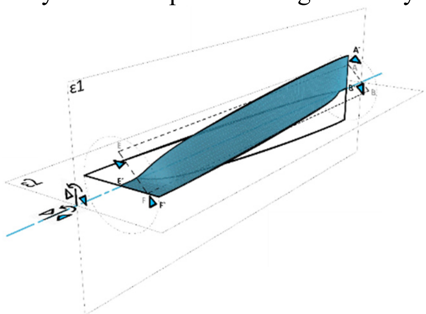

2 GEOMETRICAL PRINCIPLES OF A BEAM ELEMENT FROM 4 TORQUED STRIPS

When assembling a tube from 4 identical, thin-walled, rectangular strips (Figure 2a-e), which are hinge-joined along their longitudinal edges, a hollow, square cross-section is generated (Figure 2b), which is characterized by a 1-DOF-mechanism around its longitudinal axis. To restrain the mechanism, we can choose from several options, which among others can be cross-bracing or sidewalls at both ends of the tube. The option that we used for restraining this mechanism is to cross-wisely connect the tube`s short edges (ends) at a common seamline by deforming the four strips, as shown in Figure 2b-e. While for our purposes the connection of the individual strips along their longitudinal edges must be 1-DOF-mechanisms, the two end seamlines can be either hinge-joined or clamped. The process of closing the ends of the tube by cross-wisely connecting its short edges (Figure 2b) requires sufficient flexibility of the material and induces a twist of two times 45° in opposed directions in each of the two hinge-coupled strips (Figure 2c), a total twist of 90° of each strip as illustrated in Figures 2c-e. Consequently, the resulting geometry of the closed structural system is primarily depending on the way the tube´s ends are closed, but also affected by the scale, the width-to-length ratio of the strips, the selected material and its properties, which will be extensively discussed below. However, our proposed method of closing the tube´s ends highly efficient locks the above-mentioned 1-DOF-mechanism. A single, twisted strip usually tends to release its residual stresses by spatial deformation. By hinge-coupling four strips along their longitudinal edges, both, a 90°-torsion of each of the four individual strips, and simultaneous sideward shifts of the strips occur as shown in Figure 2 a-e and Figure 3. In the final beam element points B` and D`, as well as points E` and G` coincide by matching with the central axis of the tube, which stays unchanged in its position and which also represents the intersection line of planes $\varepsilon 1$ and $\varepsilon 2$. As illustrated in Figure 2d and 3, the planes $\varepsilon 1$ and $\varepsilon 2$ also represent the mirroring planes of the beam element. Points A`, B`, C`, D`, E`, G`, and the central axis of the tube share the (vertical) plane $\varepsilon 1$.

3 PHYSICAL MODELS AND PROTOTYPES

Our investigation is based on both, on computational simulation and analysis as well as on physical models and prototypes in various scales and materials. Early stage scaled models were made from thin sheet material including paper, cardboard, polyester, copolyester, and veneer. For larger scales and first full-scale prototypes (Figure 4, 6), different kinds of wood products were discussed and compared. Due to the desired flexibility of the material, plywood seemed to be an appropriate choice but also including aspects of sustainability and economic reasons.

3.1 *A beam element from all-birch plywood strips*

The four individual strips were made from all-birch, multipurpose plywood panels. The grains of adjoining layers are orthogonal to each other, and its volumetric mass density (including glue) is around 680 kg/m3 at relative humidity of RH 65%. The product decision for the orthotropic material, made of five plies of rotary-cut birch veneers, is based on smoothness, homogeneity of bending curvature and on its bending-strength (Metsä, 2019) (Forest Products Laboratory, 1964), as shown in Figures 4 and 6, Table 1 and explained below. The panels were intentionally cut to strips with three layers in cross direction and with two layers in longitudinal direction. According to our experience with physical models and simple material tests, the width-to-length ratio of each strip was chosen to be in the range of ≤ 1/10. Thereafter, our physical prototypes have been assembled from plywood-strips, each 2400 mm x 200 mm x 6.5 mm. Clamped at the very and at 2000 mm end, a strip-length of 400 mm is left (Figure 4) for connecting the beam during testing and to other parts of the structure as shown in Figure 1. The same width-to-length ratio has been applied to our computational simulation and analysis.

Table 1. Material properties of used all-birch plywood as provided by the manufacturer in the declaration of performance (Metsä, 2019).

Material	Thickness	Number of Plies	Approximate volume weight	Thickness tolerance
Birch-Plywood	6.5 mm	5 (3/2)	680 kg/m³ at relative humidity of RH 65%	+0.4/-0.4 mm
	Characteristic bending strength (N/mm²)	Mean modulus of elasticity in bending (N/mm²)	Characteristic compression strength (N/mm²)	Characteristic tension strength (N/mm²)
‖	50.9	12737	29.3	42.2
⊥	29.0	4763	22.8	32.8

‖ = along the face veneer grain direction ⊥ = across the face veneer grain direction

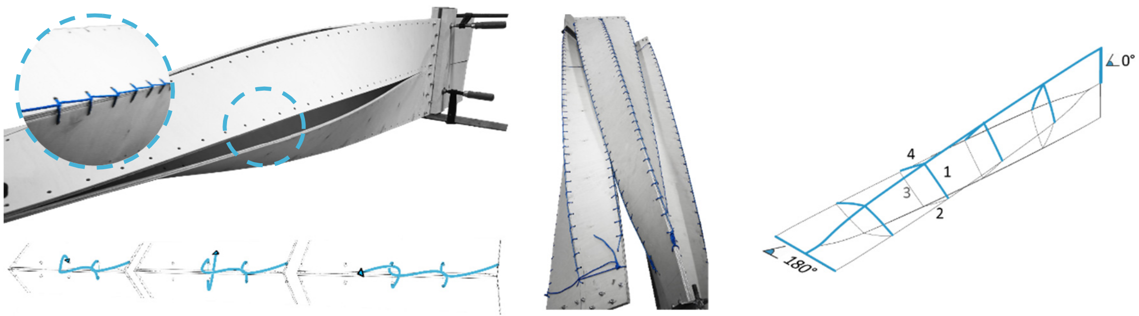

Figure 4: Lenticular openings in-between the strips before connecting by lacing technique (b) and detail of lacing by a100% multifilament, braided polypropylene (PP) rope with ø4 mm (c)
Figure 5: Clove Hitch End, a 3-step lacing/knot technique knot (a1-a3)
Figure 6: Plywood beam elements with laced seamlines
Figure 7: Changing angle (180° to 0°) along curved seamline (b)

3.2 *From crease-lines to rope-lacing to piano-hinges as seamlines*

The ease of assembly of a tube from four identical, rectangular strips is highly dependent on the way the strips are connected. Vice versa, the appropriate method of executing the seamlines is a question of scale, selection of material, associated material properties and material thickness/thinness. In our small-scale models the geometry is achieved through repetitively folding paper to create a hollow, square cross-section tube, then cross-wisely connecting the tube’s short edges, which locks the 1-DOF-mechanism. Due to negligible material thickness, the crease lines work as hinges generating the above described 1-DOF-mechanism. The problem of folding thick, rigid origami (Tachi, 2011) or folded structures from thick, hinged sheet material (Hoberman, 2010) have been widely discussed. Some of the proposed methods include offset, axis shift and trimming material at bisecting planes (Tachi, 2011), locating hinge axes in different planes (Hoberman, 2010) and spatial linkages (Chen et al., 2015).

Due to the strips´ twist of 90°, we have two aggravating conditions in addition to above-mentioned hinge-queries. Firstly, the ends of strips 1 and 4 (Figure 2a) and the central axis of the tube share the (horizontal) plane ε2 (Figures 2d and 3). This means that the angle of the seamline between strip 1 and 4 changes from 180° to 0° (Figure 7). The same applies to each successive pair of strips. Secondly, during the assembly process, the linear edges of the strips transform into the seamlines of the final beam element, which are planar curves of the (vertical) plane $\varepsilon 1$ or the (horizontal) plane ε2. The shape of the curves is also influenced by whether the seamline was clamped or hinged at the element`s ends. However, the hinges along the longitudinal seamlines have to allow for changing angles from 0° to 180° and simultaneously allow for being elastically bent as shown in Figure 7.

Techniques from making and connecting textiles have inspired architecture and engineering since history and seem increasingly interesting for construction nowadays (Fritz, 2011) (Tramontin, 2006). Sewing, weaving, knitting, stitching and lacing offer alternatives for material use and connections. In building applications these types of joints are often used in combination with other materials or connection techniques, such as the stitch and glue technique in boat building (Kulczycki, 2000). Sewing plywood asks for overlapping of the materials as it has been used in furniture making by Färg and Blanche (Färg and Blanche, 2016), and recently as sewed or as combined technique for lightweight bending active structures by ICD/ITKE (ICD, 2017) (ICD/ITKE, 2016). As examples of Godoy (Godoy, 2004) show, connecting plywood pieces by lacing only, is known in furniture production and also inspired our method for assembly (Figures 4 to 7). In the past, the first author tested and compared different patterns in terms of strength and ease of utilization with regards to the size of parts, material and material thickness. Our interests and experience in the design for rapid assembly and disassembly such as the “Z-Snap-Pavilion” - Zip assembled, bending active pavilion by coupled straight and curved line folding (Filz and Kumric, 2015) prioritized lacing as the method of choice for the first prototypes, providing the possibility of quickly closing, adjusting and reopening of lace-patterns. Another advantage of this method is the reduction of number of pieces in the joints.

In the process of assembly, the short edges of the plywood strips were connected to a thin steel plate, resulting in a clamped connection of about 5cm width. For closing the lenticular openings along their longitudinal edges (Figure 4), and for hinge-coupling the four strips, we applied the “Clove Hitch End” (Figures 4 and 5), a lacing/knot technique where the rope is fed through the pre-drilled holes on strips` edges (Figure 5) and in a second step also between itself and the plywood. This generates a crossing point, which can be transferred first by pulling against the lacing direction, followed by pulling in the lacing direction (Figure 5). Consequently, the force for closing the lenticular opening could manually be applied with ease, since our technique also relied on the friction of the rope at these points. This kind of self-locking mechanism facilitated the assembly process and did not require any knots except at the endpoints. So, the relatively low knot strength of the rope has been irrelevant, and the lenticular opening gradually closed, generating a seamline, which naturally follows its planar curve (Figures 6 and 7), but with some minor imperfections. Recent prototypes have been assembled by means of metal piano hinges, which do not conflict with the material thickness of the strips. In addition, they allow for constant change of opening-angle and have enough play for transforming from linear edges to planar curves along the longitudinal seamlines. The latest results show increased precision as well as increased structural performance, which is not fully tested and evaluated at present, and therefore not subject of this paper.

3.3 *Comparing the geometries from photogrammetry and computational simulation*

The resulting shape of the beam element from 4 torqued strips has been investigated by different means from simple measuring, to photogrammetric reconstruction, to computational simulation. The photogrammetric reconstruction of the beam element described here was done by means of RealityCapture (Capturing Reality, 2020) commercial software, which uses the Structure-from-

Motion (SfM) method and allows a cheap and easy method to record surface geometry using off-the-shelf cameras. The method is usually used for the digitization of rock surfaces (Janiszewski et al., 2020). In total, 166 RAW images of the beam were taken (Figure 8 a,b) by moving the camera around the beam at regular, spatial intervals with at least a 70% overlap between the subsequent photos. Finally, a complete dense 3D point cloud and mesh model of the beam with 40 million polygons was generated. Similar to the workflow for the photogrammetric reconstruction of rocks (Merkel, 2019), two outputs were produced, (i) a dense colored 3D point-cloud from 9 million points with a mean surface point density of 5 pts/mm2 (Figure 8d), and a high-poly textured mesh from 17.5 million polygons.

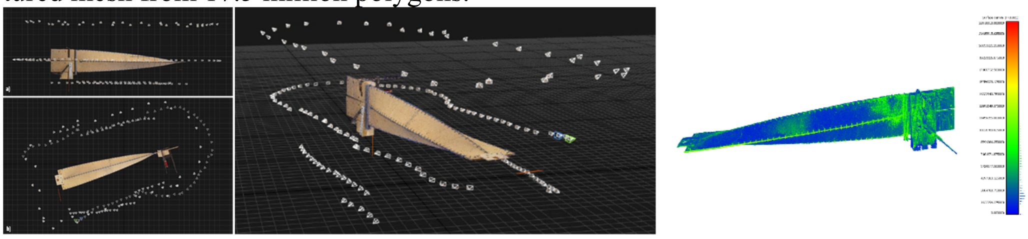

Figure 8: Side view (a), top view (b) and perspective (c) of the photogrammetrically reconstructed beam model. The surface density (d) of the 3D point cloud expressed as the number of points per square meter, calculated using a circular window of 1 mm2. The mean density equals to 4.98 points per mm2.

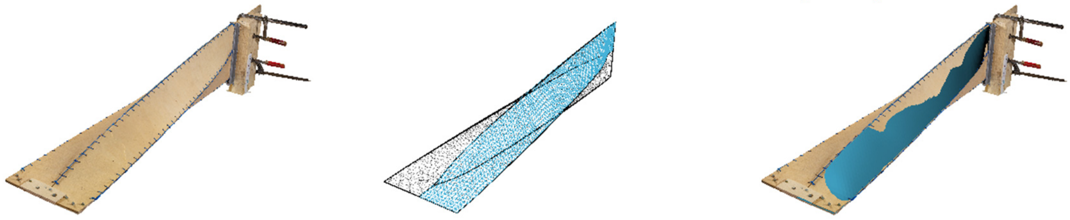

Figure 9: Photogrammetric reconstruction compared with the mesh from the computational simulation. low-poly mesh (a), mesh from computational simulation (b), overlay of low-poly mesh and mesh from computational simulation (c)

In our computational simulation each strip of the beam is generated from a mesh with 1164 control points (Figure 9b), and mesh faces of about 20 x 20 mm. The low-poly mesh from the photogrammetric reconstruction (Figures 8 and 9a) of the same strip is defined by about 165000 control points (Figure 9a). The spatial deviation of these meshes was checked by their overlay (Figure 9c), and is at a maximum of 4 mm, which is ≤60% of the strips´ thinness. The larger deviations are found at the end of the strip, whereas the center of the strip is quite precisely matching. Deviations are most probably caused by imperfections in clamping and the differences of orthotropic plywood versus isotropic aluminum in the computational model. However, the geometries match to large extend and confirm the accuracy and correctness of our computational approach. For most of the scaled physical models and full-scale prototypes where the used sheet material is thin enough, the beams showed slightly undulating strips. These undulations form a geometrical, triangular pattern and can have a stiffening effect on the element (Elmas et al., 2021). This phenomenon is also notable in our computational simulations (Figures 12, 13), to be discussed below.

3.4 *The structural performance of physical prototypes*

The above presented, laced beam element was used as a cantilevering beam in our realized kinematic (Markou et al., 2021) pavilion "Zero Gravity" (Filz et al., 2019) as shown in Figure 1. Even though the beam can be used, modified and combined in many ways (Figure 13), it was primarily tested as a horizontally cantilevering beam. We tested a beam element clamped to a fixed support by loading the free end (Figure 10 and 11). The test was set up to deliver quick results for its bending resistance, to understand the range of load bearing capacity and to learn about its deformation, displacements under load and its failure mode. The testing procedure represents a first approach, which is characterized by measuring displacements of the free end over the force (Figure 11b), which was applied by a chain hoist as uplift (Figure 10a,b) and by restricting lateral movement. The increase of force and the time and speed of loading were not fully automated, but appropriate for a first assessment of the beam's structural performance. The cantilever beam was loaded to a maximum of 2.16 kN at a displacement of 36.5 mm (Figure 11b) at the free end (see point 13 Figure 11a). The above-mentioned imperfections of the aligning of the strips at the seamlines allowed for a vertical sliding, which is at first notable at the seamline, which was under compression (Figure 10b, c). Thereafter, the beam was not further loaded, and during unloading it returned to its initial position. As a result of this very quick and rough loading test, the beam has been evaluated as reliable for its use as a structural member of the Zero Gravity pavilion and promising for future investigations. The key aspects in this regard are the beam´s self-weight of approximately 10kg compared to its structural performance and the fact that the failure mode has been neither material failure of the plywood, nor the holes for the lacing, nor the lacing or the used ropes. Vice versa, there is plenty of options for improving the aligning of the seamlines, such as using the aforementioned metal piano hinges. Present load tests are performed in a more controlled environment and larger amount of reference points collecting precise displacement data.

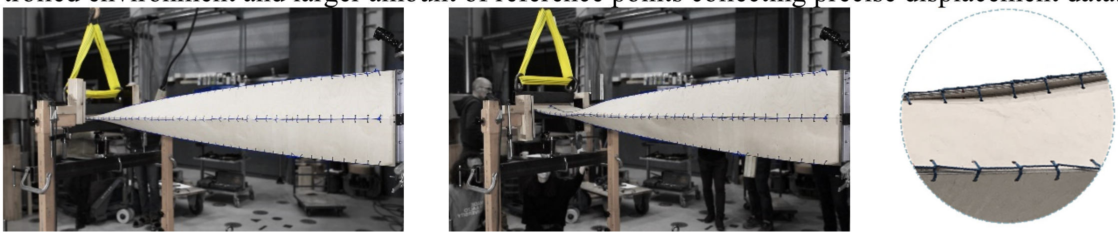

Figure 10: Test set-up with manually applied uplift by a chain hoist at the free end of the beam (a), and failure mode due to imperfection at the seamline in compression (on top due to uplift) (b), detail (c)

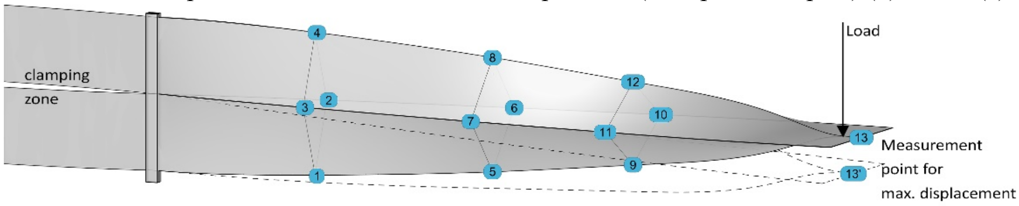

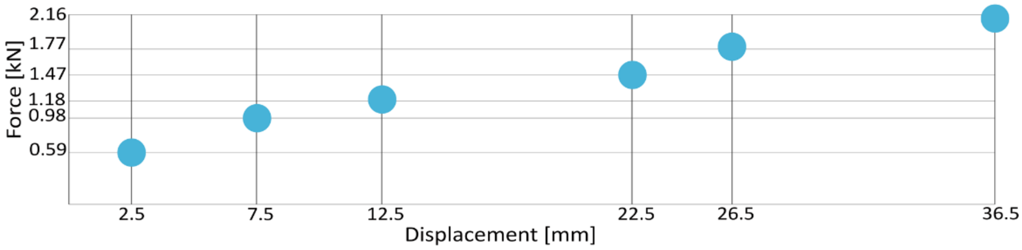

Figure 11: Test set-up for the cantilevering beam (a); load/displacement data at the free end (b)

4 COMPUTATIONAL SIMULATION

4.1 *Structural analysis*

For reasons of symmetry, only one strip is considered in the numerical simulations, in order to reduce the computational cost. More specifically, a single strip from isotropic aluminum (Table 2), is clamped to one end. The dimensions of the strip are equivalent to the above-described, physical prototype. Two rigid regions are introduced to the initial strip from 0 to 50 mm and from 1950 mm to 2400 mm, so that the final length of the strip is 2000 mm and the final width to length ratio is equal to 1/10. In this way the clamped-clamped connection of the four strips is represented, and one longitudinal edge of the strip is forced to move within a horizontal plane, while the other one is forced to move within a vertical plane as shown in Figure 3. The strip was simulated by means of a deformable shell element represented by a mesh of 20 mm x 20 mm in Abaqus/CAE 2020 (Dassault_Systèmes, 2020). The strip was subjected to quasi-static analysis (Clough and Penzien, 1993), during which a rotation of 90° along with a horizontal and vertical displacement equal to half of strip's width were imposed. As mentioned in section 3.4 the geometry of the simulated mesh coincided with the mesh from the photogrammetric reconstruction, with a deviation of ≤60% of the material thickness. The von Mises stresses and geometry of the single deformed strip are shown in Figure 12. As it can be seen from the distribution of stresses, at the ends of the strip the stresses are approaching the ultimate yield stress (324MPa) of the aluminum.

Table 2. Material properties of Aluminium – material properties

Mass density	Young Modulus	Poisson Ratio	Plastic Strain	Initial Yield Stress	Ultimate Yield Stress
2.7(g/cm3)	70000(MPa)	0.33	0.2	276(MPa)	324(MPa)

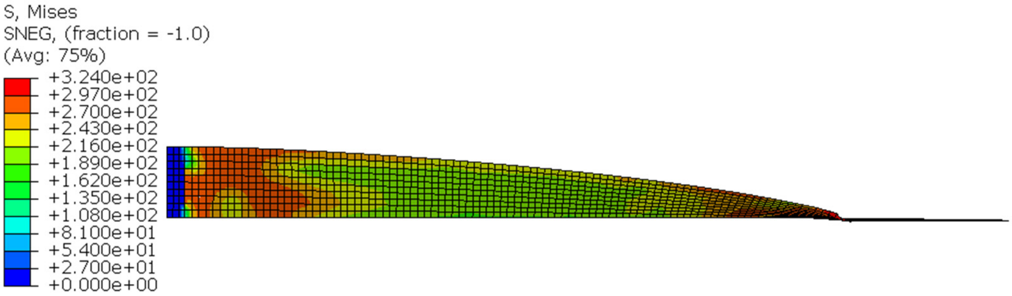

Figure 12: Von Mises stresses of a single strip in sideview

4.2 *Parametric study and analysis*

To investigate the buckling phenomenon of the strip's surface that has been observed in the early paper models, a parametric study has been performed by using quasi-static analysis with the material thickness as variable ranging from 6.5 mm to 0.5 mm. The first signs of buckling of the strip started around 2.4 mm. In Figure 13 (right), overlays of longitudinal sections illustrate the local buckling according to material thickness by comparing the strips´ material thickness with 2.4 mm (yellow) and 0.5mm (magenta) with 6.5 mm (blue), where no local buckling was observed. For analyzing and comparing the surface, the Zebra patterns of the three strips were examined (Figure 13 left). The Zebra pattern is a surface analysis command provided by the software Rhinoceros (McNeel, 2010), which visually evaluates surface properties such as smoothness and continuity by using a stripe map. The Zebra pattern does not only highlight the differences of the surfaces according to the material thickness, but it shows especially at 0.5 mm material thickness (magenta) undulations, which form a triangular pattern. What is depicted in Figure 13 are the different buckling modes of the torqued strip. As the material becomes thinner the structure buckles in a different mode in order to find a new stable configuration.

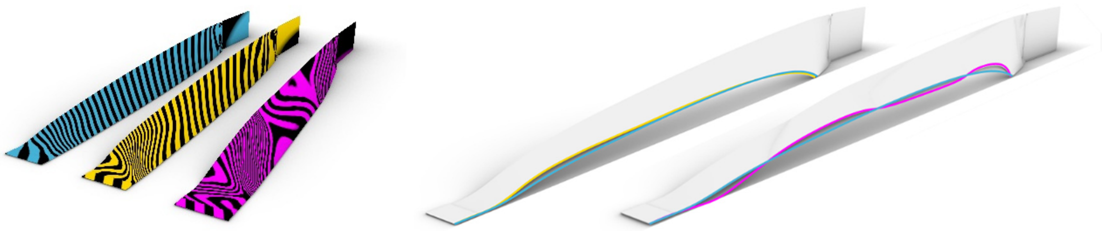
Figure 13: (left) Utilization of Zebra patterns of the three strips for analyzing and comparing the surface of the following strips: blue = 6.5 mm, yellow= 2.4 mm, magenta = 0.5 mm (with undulations forming a triangular pattern); (right) Longitudinal sections overlay illustrating the local buckling according to material thickness; blue = 6.5 mm, yellow= 2.4 mm, magenta = 0.5 mm

5 CONCLUSIONS AND OUTLOOK

Twisted elements and structures have been realized many times throughout architectural history. Besides the aspects of architectural design and aesthetics, usually torsion is not considered beneficial for both, the material and structural aspects, even though in some cases a structural benefit might be inherent. As such an example, the structural geometry of a beam element from 4 torqued strips, is presented in this paper. Our methods of investigation and comparison of geometrical and structural aspects include physical prototypes, photogrammetric reconstruction and computational simulation. The overlay of generated meshes shows a spatial deviation, which is ≤60% of the strips´ thinness. These results confirm that our computational approach is matching the full-scale, physical prototype at high precision. The loading capacity tests of the beam are in an early stage, but it has been evaluated as reliable for its use as a structural member of the Zero Gravity pavilion and as promising for future investigations. The used lacing techniques and increased precision in aligning of the seamlines and assembly of the beam element will lead to excellent structural performance, especially when compared to its self-weight. Very thin strips have notably undulating surfaces, a local buckling behavior already observed in scaled, physical models and later investigated in a parametric study. This phenomenon can have a geometric stiffening effect to the beam as explained in (Elmas et al., 2021). Altogether, the shapes that we generated by using torsion as a design driver, can be both highly efficient in material use and structural performance. Paralleled with the ease of fabrication and assembly, this opens new avenues for the design of lightweight structures, first explored by the realized Zero Gravity pavilion.

REFERENCES

Ayers, A. (2004) *The Architecture of Paris: An Architectural Guide*, Edition Axel Menges.

Capturing Reality, S. R. O. (2020) RealityCapture: Mapping and 3D Modeling Photogrammetry Software.

Chen, Y., Peng, R. & You, Z. (2015) APPLIED ORIGAMI. Origami of thick panels. *Science (New York, N.Y.),* 349**,** 396.

Clough, R. W. & Penzien, J. (1993) *Dynamics of Structures*, McGraw-Hill.

Cornet, A. G. Y. (1970) *Cripta de la colonia güell*, Poligrafa.

Dassault_Systèmes (2020) Abaqus Unified FEA - SIMULIA™. Dassault Systèmes

Elmas, S., Filz, G. H., Markou, A. A. & Romanoff, J. (2021) Zero Gravity: a novel cantilever beam utilizing elastic torsion for structures and architecture.

Färg, F. & Blanche, E. M. (2016) COUTURE armchair.

Filz, G. H., Elmas, S. & Markou, A. (2019) Zero Gravity 2.0 Exhibition | Aalto University.

Filz, G. H. & Kumric, I. (2015) "Z-Snap-Pavilion" - Zip assembled, bending active pavilion by coupled straight and curved line folding. *IASS Symposium 2015 "Future Visions"*.

Forest Products Laboratory, U. S. D. O. A. (1964) The bending strength and stiffness of plywood. Madison, Wis. : U.S. Dept. of Agriculture, Forest Service, Forest Products Laboratory.

Fritz, S. (2011) The Very Fabric of Architecture: textile use in construction.

Fuchs, A. (1951) Die Spiralsäule in der Kunstgeschichte. *Westfalen - Hefte für Geschichte, Kunst und Volkskunde. Mitteilungen des Vereins für Geschichte und Altertumskunde Westfalens, des LWL-Landesmuseums für Kunst und Kulturgeschichte, des LWL-Amts für Denkmalpflege in Westfalen und des LWL-Museums für Archäologie 29 1951*.

Godoy, E. (2004) Knit Chair. *emilianogodoy.com.*

Hoberman, C. (2010) Folding structures made of thick hinged sheets.

Holmes, D. P. (2020) *Mechanics of Materials: Torsion*.

Icd (2017) ICD Sewn Timber Shell 2017.

Icd/Itke (2016) ICD/ITKE Research Pavilion 2015-16.

Janiszewski, M., Uotinen, L., Baghbanan, A. & Rinne, M. (2020) Digitisation of hard rock tunnel for remote fracture mapping and virtual training environment. *ISRM International Symposium Eurock 2020 - Hard Rock Engineering.* Trondheim, Norway.

Kulczycki, C. G. (2000) Method for building lapstrake boats.

Markou, A. A., Elmas, S. & Filz, G. H. (2021) Revisiting Stewart–Gough platform applications: A kinematic pavilion. *Engineering Structures,* 249**,** 113304.

McNeel, R., Associates (2010) Rhinoceros 3D. Seattle, WA.

Merkel, J. (2019) Utilization of photogrammetry during establishment of virtual rock collection at Aalto University.

Metsä, W. (2019) Metsä Wood Declaration of Performance Library - NO. MW/PW/411-001/CPR/DOP. 02020 Metsä, Finland, METSÄ WOOD.

Tachi, T. (2011) Rigid-Foldable Thick Origami. *Origami 5.* A K Peters/CRC Press.

Tomlow, J. (2004) Matching Nature With 'Complex Geometry'–An Architectural History. IN Brebbia, C. A., Sucharov, L. J. & Pascolo, P. (Eds.) *Design and nature.* WIT Press.

Tramontin, M. (2006) Textile Tectonics: An Interview with Lars Spueybroek.

Tronzo, W. (2005) *St. Peter's in the Vatican*, Cambridge University Press.

Werner, F. R. (2009) *Coop Himmelb(l)au, BMW-Welt, München,* Stuttgart / London, Edition Axel Menges.

Wise, C. (2016) *Part 2 - Designing a meaningful structure*, IStructE Ltd - The Institution of Structural Engineers.